Lehrstuhl für Bildverarbeitung
Institute of Imaging & Computer Vision

Approaches for High-Speed Melt Pool Detection in Laser Welding Applications

Nicolaj C. Stache*, Henrik Zimmer*, Jens Gedicke#, Boris Regaard#, Alexander Olowinsky#, Achim Knepper*, and Til Aach*

*Institute of Imaging and Computer Vision
RWTH Aachen University, 52056 Aachen, Germany
tel: +49 241 80 27860, fax: +49 241 80 22200
web: www.lfb.rwth-aachen.de

#Fraunhofer Institut für Lasertechnik,
Steinbachstr. 15, D-52074 Aachen, Germany
phone: + (49) 241 89060, fax: + (49) 241 8906121
web: www.ilt.fraunhofer.de

in: Vision, Modeling, and Visualization (VMV) 2006. See also BibTeX entry below.

BibTeX:

```
@inproceedings{STA06b,
   author    = {Nicolaj C. Stache and Henrik Zimmer and Jens Gedicke and Boris
                Regaard and Alexander Olowinsky and Achim Knepper and Til Aach},
   title     = {Approaches for High-Speed Melt Pool Detection in Laser
                Welding Applications},
   booktitle = {Vision, Modeling, and Visualization (VMV) 2006},
   address   = {Aachen},
   month     = {November 22-24},
   year      = {2006},
   pages     = {217--224}}
```


document created on: June 15, 2007
created from file: Laser7deckbl.tex
cover page automatically created with CoverPage.sty
(available at your favourite CTAN mirror)

RWTH AACHEN
RHEINISCH-WESTFÄLISCHE TECHNISCHE HOCHSCHULE AACHEN

Approaches for High-Speed Melt Pool Detection in Laser Welding Applications

Nicolaj C. Stache*, Henrik Zimmer*, Jens Gedicke#, Boris Regaard#, Alexander Olowinsky#, Achim Knepper*, and Til Aach*

*Institute of Imaging and Computer Vision, RWTH Aachen University, D-52056 Aachen, Germany
phone: + (49) 241 8027860, fax: + (49) 241 8022200
Email: {Stache, Zimmer, Knepper, Aach}@lfb.rwth-aachen.de
#Fraunhofer Institut für Lasertechnik, Steinbachstr. 15, D-52074 Aachen, Germany
phone: + (49) 241 89060, fax: + (49) 241 8906121
Email: info@ilt.fraunhofer.de

Abstract

In this paper several approaches for the detection of the melt pool circle (i.e. its position and radius) in laser welding applications are described. Instead of indirectly examining the evolution of the melt pool via the radiation of plasma that is generated during the welding process, we use a direct view onto the melt pool that is possible in a narrow wavelength band with a coaxial aligned high speed CMOS imaging sensor. Since visual inspection is often a bottleneck in mass production, we focus on high speed approaches that enable real-time monitoring of the melt pool parameters.

1 Introduction

Only a short time after its discovery in 1961, lasers were tried for use in material processing. The main advantage compared to conventional methods for material processing is that no mechanical contact to the workpiece is necessary. Another benefit especially for welding is that a very narrow but deep weld seam in combination with a high welding speed can be achieved, making both high accuracy and high performance possible [4, 1].
Thanks to that, a wide area of industrial and medical applications stands open to use of lasers: Conventional welding processes were increasingly substituted by laser welding and new applications became possible with lasers.
Examples for applications of laser welding are found in the automotive industry where a reduction of weight in combination with an increase of stability could be achieved with the use of laser cut and laser welded tailored blanks. Another field of application is precision engineering, where the demand of high accuracy and narrow seams make the use of lasers vital.
The principle of a laser welding process is shown in Figure 1: The beam is focussed to a point with a radius of a few tenths of a millimetre. A resulting intensity of $10^6\,\mathrm{W/cm^2}$ evaporates the material and builds a capillary – the so called keyhole. Due to that keyhole, the beam can penetrate deeper into the workpiece and achieves particularly deep and narrow seams [1].

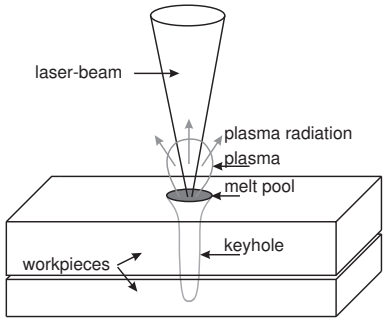

Figure 1: Principle of laser beam welding

However, laser welding is a very complex and highly dynamic process and is thus vulnerable to process errors. To maintain the exactness in combination with a high productivity it is indispensable to accurately control the welding process.
There are several possibilities to monitor the

welding process in order to control it. Most of them are based on the fact that plasma is generated when the laser interacts with the material (see Figure 1). The radiation of this laser induced plasma is often measured with a spatially integrating photo detector (usually a photo diode) with optical filters to limit the detected radiation to a certain spectral range. It contains much information about the laser, the status of the material and the stability of the welding process.

Since changes in the plasma may last only fractions of a millisecond, the high achievable sampling rate of simple photo detectors is beneficial. In recent years an extended version of this approach became common practise: The quality of the monitoring results could be significantly increased by the use of imaging systems with two-dimensional spatial resolution [2, 8, 7].

Figure 2 shows a setup to monitor the laser welding process with a high speed camera. Here, the optical path of the camera runs coaxial to the path of the laser radiation. This constellation is called *Coaxial Process Control* (CPC). A dichroit that lets the laser beam pass through but reflects radiation (in a certain interval of wavelengths) for process monitoring, directs the visual information onto the camera. In this commonly used constellation the camera captures the radiation of the plasma.

The melt pool is thus assessed only indirectly through the plasma radiation. However, to accurately measure the welding parameters such as radius and position of the melt pool – the objective of this contribution – a direct view of the melt pool is needed.

Since the radiation of the plasma is quite low for wavelengths between 800 nm and 850 nm, it is possible to capture the melt pool instead of the plasma using an illuminating light source with wavelengths precisely in this interval. In this case a beam splitter has to be placed in the path of the camera to introduce the additional radiation. In addition, a filter is placed in front of the camera optics, which lets only wavelengths in the specified interval of 800 nm to 850 nm pass, thus preventing plasma radiation from reaching the camera. Instead, frames can be captured that show a direct view onto the melt, without any influence of plasma radiation [13]. The qualitative comparison between an image without (Figure 3a) and with additional illumination (Figure 3b) underlines the benefits of the direct view onto the melt pool.

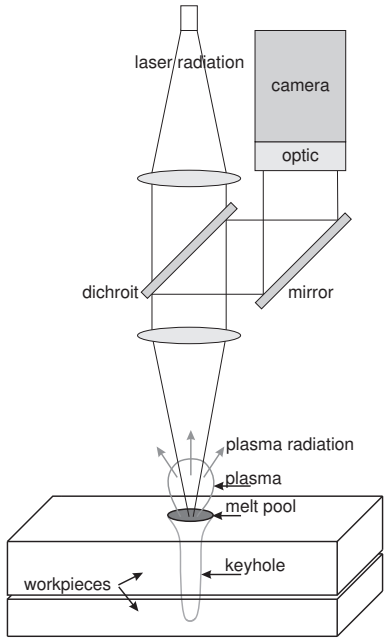

Figure 2: Process monitoring via CPC-system [9]

We focus here on the high-speed detection of the position and the radius of the melt pool. As already mentioned, changes in the plasma may only last a few fractions of a millisecond – this also applies to the melt pool. The frame rate needed for melt pool monitoring may therefore be as high as 5000 fps. Although laser welding systems can currently not be controlled at such short time intervals, the cycle times for laser welding of about 250 milliseconds still require that a processing speed of about 400 fps be reached. In addition, the length of the laser pulse – about several ten milliseconds – needs to be counted from the point in time when the laser actually starts to interact with the material, i.e., the beginning of the melt pool formation. Detection of this moment requires frame rates of 1000 fps and more. Thus the demand of high speed melt pool analysis may not be satisfied with standard algorithms used in video processing.

The challenge here will be to find a method that makes a good compromise between high speed and robustness to sputter and noise.

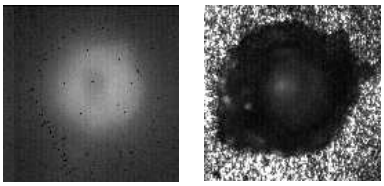

(a) (b)

Figure 3: Images of a melt pool: via plasma radiation without additional illumination (a), and with additional illumination (b), where the plasma radiation was filtered out. The melt pool appears as a dark, disk-shaped region in cluttered background.

The paper is organized as follows: In section 2 a very robust but computationally relatively expensive method is developed to detect the melt pool size and position. In section 3 the method will be modified towards higher throughput. A comparison of the two approaches is carried out in section 4. Conclusions are drawn in section 5.

2 Melt pool detection by fast correlation

Figure 4 shows some typical samples of melt pool evolution during a welding process. Two layers of copper (type: K55, thickness top side: 0.2 mm, bottom side: 0.6 mm) were welded with a Nd:YAG laser with 1.4 kW and a pulse length of 20 ms. The diameter of the focal point is 0.3 mm and the field of view covers $0.8 \times 0.8\,\mathrm{mm}^2$. The sequence is recorded with a high speed camera with 128×128 pixels at 5000 frames per second, the scene is illuminated with a diode laser with a wavelength of $\lambda = 830\,\mathrm{nm}$.

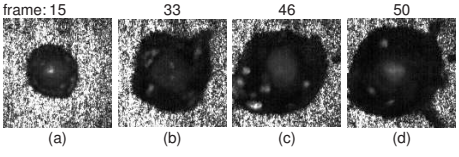

Figure 4: Melt pool evolution in a welding process

Evidently, in Figure 4(a) the shape of the melt pool is well approximated by a dark circular disk on irregular bright background. Towards higher frame numbers (Figure 4(b) – (d)) the diameter of the melt pool increases and its shape becomes more irregular due to sputter and the strong movement in the melt as a result of thermal processes [12]. Furthermore, bright reflections occur in the melt.

The detection of the melt pool parameters radius and position should be done without being influenced by reflections or sputters, i.e. sputters should not count as melt pool area. Thus, an approach to simply detect the size of the dark area may not be applicable.

An alternative is the use of the Hough transform [5, 6] to detect the circular disk of the melt pool. The advantage is that the Hough transform can be used to directly find the parameters of shapes that may have regular boundings, such as circles. Thus it can easily distinguish between clutter, like circles induced from sputter, and the circle belonging to the melt pool using prior knowledge about radius and position. A major drawback is that the classical Hough transform is computationally expensive: First, the image has to be prefiltered to find edges, then the accumulator has to be filled and the maximum for the best fit has to be found. The high computational effort of this brute force approach relative to the high demand on high throughput make the use of the Hough transform impractical.

Thus a method has to be developed that is as robust as the Hough transform but requires less computational effort. For reason of efficiency, the new approach should work without previous filtering such as edge detection. With respect to the reflections in the melt pool and the noisy background the new approach should be based on spatial integration to achieve high robustness. One possibility to meet these requirements is as follows:

Each captured frame is matched to a set of idealized binary prototype melt pool images with varied but defined parameters. The best match then leads directly to the sought parameters. This procedure is very similar to cross correlation computation [10],

$$r_{xy}(\mathbf{k}) = \sum_{\mathbf{n}} x(\mathbf{n}) \cdot y(\mathbf{n}+\mathbf{k}) \qquad (1)$$

where $r_{xy}(\mathbf{k})$ denotes the cross correlation function of two image signals $x, y \in \mathbb{R}^2$ over shift $\mathbf{k}$. The maximum of $r_{xy}(\mathbf{k})$ specifies the position where both signals are most similar – transferred to melt pool images, this straightforward form of cross correlation determines where a given melt pool prototype with a specified radius fits best to a live frame.

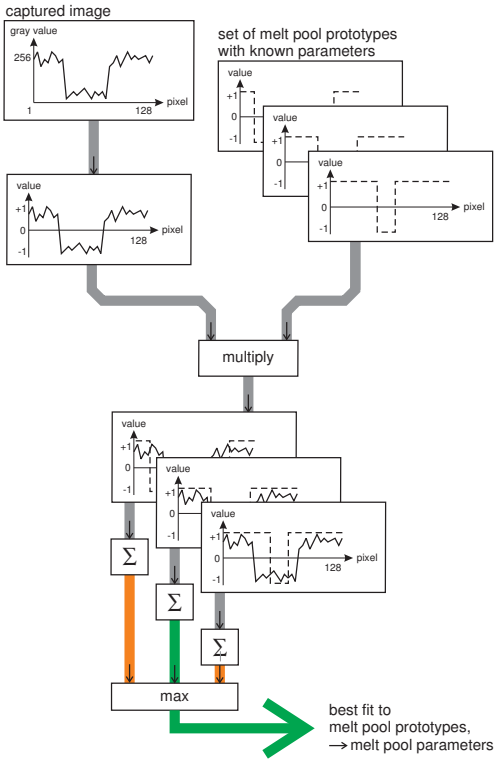

Figure 5: Diagram of robust melt pool detection

To also determine the melt pool prototype with the best fitting radius, we subtract the mean values from both the live and prototype images. The pointwise multiplication of live image and prototype in (1) then yields the more positive coefficients, the better the fit between live image and prototype. The algorithm is depicted in Figure 5.

For reasons of clarity, only one-dimensional signals (in this case slices through the image's centre) are depicted. The generation of the melt pool prototypes is done offline before the welding process starts; optionally, these may be normalized to range between $[-1, 1]$. First, the mean value is subtracted from the frame to be analyzed. The frame to be analyzed is then multiplied pixelwise with each prototype and summed up. In the last step, the best-fitting prototype is found as the one maximizing the sum.

The computational effort of the described approach mainly depends on the number of comparisons or correlation computations that have to be carried out to determine the melt pool parameters. Hence, it is

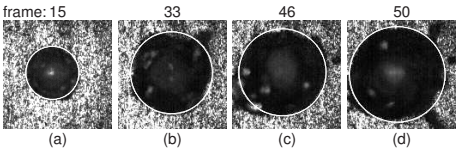

Figure 6: Melt pool peripheries detected by fast correlation.

reasonable to reduce the amount of comparisons by exploiting prior knowledge of the process. One aspect is that the variation of the melt pool position between two frames is rather low. Another aspect is that the melt pool circle generally increases during the welding process. Compared to a full search, the number of correlation computations can thus be reduced by limiting the search for both radius and position of the melt pool in a new frame to small intervals around their values in the previous frame. As an example, limiting this range to ± 8 pixels for the position and to -5 . . . +20 pixels for the radius implies 7514 correlation computations instead of over 2.6 million for a full search. Figure 6 shows the results obtained with these assumptions. The white circles fit well to the periphery of the melt pool. The detection speed can be increased even further when the number of comparisons decreases as shown in section 4. Actually, 200 comparisons suffice when a smooth reaction to changes is desired. In this case a frame rate of 9.2 fps can be achieved with a 3 GHz personal computer and compiled Matlab code. Further opportunities for speed up, such as multi-scale approaches or gradient based search is part of our current work.

3 Melt pool detection by fast boundary point analysis

In section 2 a robust method that obtains good results for circle fitting was introduced. However, for applications with short cycle times its processing speed on a standard personal computer is by far not sufficient. One approach for speed up was the use of prior knowledge that has helped to reduce the number of comparisons or correlation computations to the set of melt pool prototypes.

Another aspect of prior knowledge has been ignored up to now: Since we have knowledge of the sought shape this information could be used to

reduce computational effort, too.
To fully describe a circle, three known points lying on its periphery suffice. Thus, for a complete analysis of the melt pool the analysis of three regions is sufficient.
One approach to determine the sought parameters is to simply sum up the pixel values in each region and to infer from that sum and the regions' position the radius and location of the melt pool. The advantage of this method is its low complexity and low computational effort. The major drawback making it impractical for use is that it depends strongly on the actual grey levels of melt pool and background, which are unknown and may vary. While the influence of this effect could be mitigated by binarizing the image, the threshold itself would also be highly dependent on the material colour and lighting, thus only shifting the problem.

One solution of that problem is given by the approach in section 2: Since we just seek to locate three points defining the circle's periphery, it suffices to apply one-dimensional versions of the above correlation in small regions through which the circle can be expected to pass.
Figure 7 illustrates this for the case of using four regions: It schematically shows an image of a melt pool after subtraction of its mean and grey level normalization, and with a coordinate system centred in the image centre. The four mentioned regions denoted by N, S, E, W cover a line of one pixel width from the centre to the edge of the image; the assigned counts are the (unknown) numbers of melt pool pixels in each region.
To determine the numbers of melt pool pixels in each region, only four one dimensional correlations have to be computed: An efficient method for implementation is shown exemplarily for the regions E and S in Figure 7. First, the line shaped region with the length n is replicated within a $(n+1) \times n$ matrix. Then it is multiplied component-wise with a previously generated triangular matrix composed of one-dimensional prototype slices through the melt pool. Subsequently, we calculate row-wise sums. The position-index of the maximum entry in the sum vector is identical to the number of melt pool pixels plus one in this region.
Thus, for each region the position of the melt pool boundary can be determined – that means the constellation in Figure 7 provides four points for circle

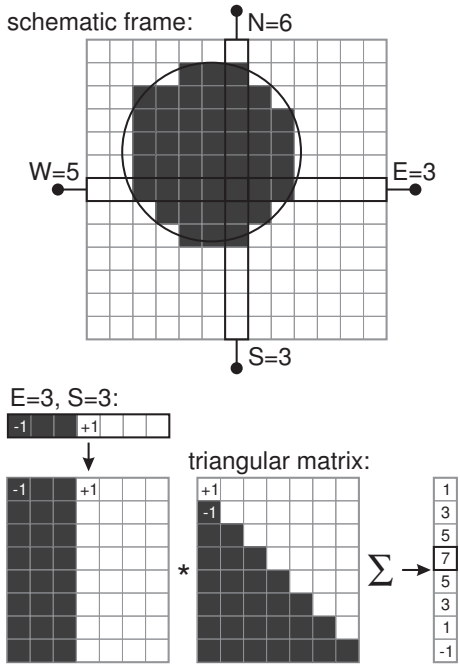

Figure 7: Fast boundary point analysis using correlation of small regions N, S, E, W with a triangular matrix (i.e. a set of steps)

detection.
The next step is to compute the circle centre and radius from its detected boundary points. In this paper two alternative possibilities will be discussed: The direct algebraic calculation of one circle from the melt pool points and alternatively, a method to fit one circle to the detected points using a least squares approach.

Direct algebraic calculation Considering the example given in Figure 7, four periphery points N, S, E, W are used to characterize the melt pool circle – so 4 combinations (NSW, NSE, NEW, and SEW) are possible to determine the melt pool parameters. In general, the number of combinations c may be calculated for m available points on the periphery as [11]

$$c = \binom{m}{3} . \tag{2}$$

NSW	NSE	NEW	SEW
N	N	W	W
S	S	E	E
W	-E	N	-S
x	x	y	y
y	y	x	x
r	r	r	r

Table 1: Interchange-scheme

For a given combination, say NSW, the melt pool parameters ($x,\ y,\ r$) may be calculated as follows with respect to the centre of the image:

$$r = \frac{1}{2}\sqrt{\mathrm{N}^2 + \mathrm{S}^2 + \mathrm{W}^2 + \left(\frac{\mathrm{N}\cdot\mathrm{S}}{\mathrm{W}}\right)^2} \quad (3)$$

$$x = \pm\sqrt{r^2 - \left(\frac{\mathrm{N}+\mathrm{S}}{2}\right)^2} \quad (4)$$

$$y = \frac{\mathrm{N}-\mathrm{S}}{2} \quad (5)$$

The ambiguity in (4) can be resolved by comparing W and r: if W is greater than r, x is negative, otherwise x is positive.

For the other combinations circles can be computed simply using equations (3)–(5) but the variables have to be interchanged as shown in Table 1.

In idealized melt pool images the calculation of circles from different combinations of periphery points should yield identical results. Real sequences are afflicted with sputter, reflections in the melt and noise so the computed circles may differ. Hence the best fitting circle has to be picked. For this selection many procedures are possible: One method is to consider the circles in the parameter space to find the best fit: a straightforward approach is to pick the circle that has the smallest Euclidean distance to the circle determined in the previous frame. Section 4 shows some results obtained with this method. An alternative to find the optimal parameters is to compare the circles based on correlations of melt pool prototypes to the whole image as described in section 2. Combinations with a least-squares approach or the use of a predictor are promising, too. A detailed comparison of that methods will be part of our future work.

Least squares approach Another possibility to directly use the four determined points of the circle's boundary line is least-squares fitting of the algebraic distance as proposed in [3]. Starting from the representation of a circle in the plane

$$a\mathbf{x}^T\mathbf{x} + \mathbf{b}^T\mathbf{x} + c = 0\,, \quad (6)$$

where $a \neq 0$ and $\mathbf{x}, \mathbf{b} \in \mathbb{R}^2$ the equation may be transformed to

$$\left(x_1 + \frac{b_1}{2a}\right)^2 + \left(x_2 + \frac{b_2}{2a}\right)^2 = \frac{\|\mathbf{b}\|^2}{4a^2} - \frac{c}{a} \quad (7)$$

and thus yielding centre and radius:

$$\mathbf{z} = (z_1, z_2) = \left(-\frac{b_1}{2a}, -\frac{b_2}{2a}\right) \quad (8)$$

$$r = \sqrt{\frac{\|\mathbf{b}\|^2}{4a^2} - \frac{c}{a}}\,. \quad (9)$$

The coefficients a, $\mathbf{b}$ and c are computed from the detected periphery points. If we insert these coordinates in (6) we obtain a linear system of equations $\mathbf{Bu} = \mathbf{0}$ with

$$\mathbf{B} = \begin{pmatrix} x_{11}^2 + x_{12}^2 & x_{11} & x_{12} & 1 \\ \vdots & \vdots & \vdots & \vdots \\ x_{m1}^2 + x_{m2}^2 & x_{m1} & x_{m2} & 1 \end{pmatrix} \quad (10)$$

and $\mathbf{u} = (a, b_1, b_2, c)^T$. In addition, we use the constraint $\|\mathbf{u}\| = 1$ to prevent obtaining the trivial solution. This leads to a standard problem $\|\mathbf{Bu}\| = \min$ subject to $\|\mathbf{u}\| = 1$ that is equivalent to finding the right singular vector associated with the smallest singular value of $\mathbf{B}$. As mentioned above, we use the minimization of the algebraic distance for least squares fitting. The advantage of this approach is its simplicity compared to minimizing the geometric distance that has to be done iteratively. In general the disadvantage is the uncertainty to what is minimized in geometrical sense (e.g. curvature bias) [3, 14].

In our application, however, of circle fitting to periphery points detected in reasonably spread regions, experiments have shown good results by minimizing the algebraic distance.

4 Results

This section illustrates the performance of the three discussed methods and hints at problems that may occur in practice. Figure 8 shows some results for the images in Figure 4 obtained with different methods: #1 is the approach proposed in section 2 with

a set of 200 comparisons or correlation computations for each frame. The results are almost identical to those with 7514 correlation computations but the computed circle needs several frames to follow heavy jumps in radius or position. Thus a kind of "slope overload" results from too small the parameter search ranges. Compared to the other images the results obtained with this approach look best and the radii are closest to ground truth (see Figure 9) but unfortunately, the frame rate is only 9.2 fps as discussed.

The second method #2 – introduced in section 3 – calculates 4 circles using the periphery points N, S, E, W and picks the circle that is closest in parameter space to the previously determined one. The computational effort is quite low; frame rates of about 2100 fps can be realized with a standard PC and compiled Matlab code. In direct implementation in C++ or Assembler, an additional speed up is expected. As shown in Figure 9, this approach exhibits stronger deviations to ground truth towards higher frame numbers. Methods #2 and #3 are more vulnerable to clutter because the size of integration (i.e. the size of the regions within which periphery points are sought) is relatively small compared to method #1 where it covers the whole image, thus reducing the strong influence of clutter such as melt pool reflections. Furthermore the selection rule in method #2 is vulnerable to error propagation. If one circle detection is disturbed e.g. by melt pool reflections, in the next frame a circle is chosen that is most similar to the previously detected erroneous result. In general, method #3 shows better results at high frame rates of about 1600 fps, only a few radii are erroneous due to melt pool reflections.

To improve robustness of methods #2 and #3, it is recommended to make the methods insensitive to melt pool reflections e.g. by use of prior knowledge (predictor) or temporal median filtering. Another approach we will examine in near future is the use of more regions across the circle periphery to increase robustness and to find out which one of the extended approaches forms the best compromise between detection speed and robustness.

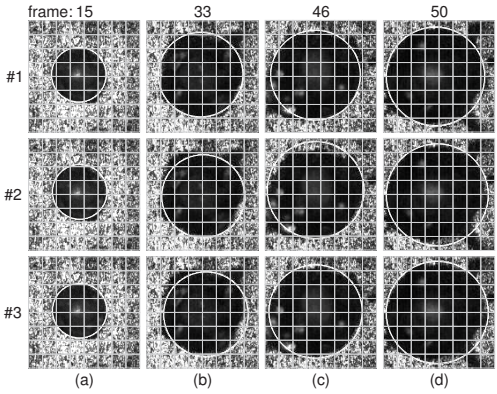

Figure 8: Melt pool circles obtained with three different methods:
#1: comparison to a set of melt pool prototypes (section 2) 9.2 fps, #2: periphery-point based method: pick the circle that has the smallest Euclidean distance to the previous picked one, 2177.5 fps, #3: periphery-point based method: minimize the algebraic distance – least squares approach, 1595.3 fps

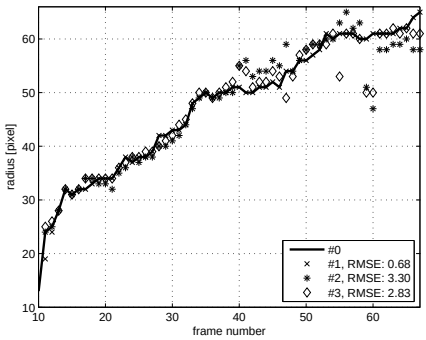

Figure 9: Determined radii (sequence from Figure 4), #0: ground truth, #1, #2, and #3 correspond to Figure 8, RMSE: Root Mean Squared Error in pixels.

5 Conclusions

In this paper mainly three procedures were discussed to estimate the melt pool parameters size and position: A robust method where each captured

frame is compared with a set of melt pool prototypes, and two methods exploiting the fact that the melt pool circle may be computed from at least 3 known boundary points. The major challenges for the detection were the high frame rates and the desired robustness to noise, sputter and discontinuities in the melt pool's boundary.

Experiments have shown that processing at high frame rates such as 2100 fps for melt pool detection are possible even with a standard personal computer and compiled Matlab code. Further speed up is expected with the direct implementation in C++ or Assembler and will be part of our future work. It is expected that detection speed will be sufficient to allow online-control of the laser welding process with the detection of melt pool radius and position at even highest cycle times in near future.

Another aspect of our future research will be the examination of different approaches to increase robustness, such as the use of more boundary regions or the suppression of sputter and melt pool reflections. Furthermore a detailed comparison of the different approaches will be carried out in near future.

6 Acknowledgements

This work is funded by the collaborative research project "INTAKT" in the funding program "InnoNet" from the German Federal Ministry of Economics and Technology (BMWi) with VDI/VDE-IT. The authors gratefully acknowledge this support as well as the active cooperation of all project partners.

References

[1] A. Bollig, S. Mann, R. Beck, and S. Kaierle. Einsatz optischer Technologien zur Regelung von Laserstrahlschweißprozessen. *Automatisierungstechnik*, 53:513–521, 2005.

[2] J. Fang, Y. Chen, L. Li, and L. Wu. Coaxial monitoring with a CMOS camera for CO_2 laser welding. In *Light-Emitting Diode Materials and Devices. Proceedings of the SPIE*, volume 5633, pages 101–109, Beijing, China, 2005.

[3] W. Gander, G. H. Golub, and R. Strebel. Least-squares fitting of circles and ellipses. In *BIT*, 34, pages 558–578, Springer Netherlands, 1994.

[4] G. Herziger and P. Loosen. *Werkstoffbearbeitung mit Laserstrahlung*. Hanser, München, 1993.

[5] Paul V. C. Hough and Ann Arbor. Method and means for recognizing complex patterns. *United States Patent and Trademark Office*, 3069654, 1962.

[6] B. Jähne. *Digitale Bildverarbeitung*. Springer, Berlin, 2002.

[7] S. Kaierle, P. Abels, G. Kapper, C. Kratzsch, J. Michel, W. Schulz, and R. Poprawe. State of the art and new advances in process control for laser materials processing. In *Proceedings of the 20th ICALEO*, volume 90, pages 1012–1022, Jacksonville, Florida USA, Oct. 15-18 2001.

[8] M. Kogel-Hollacher, C. Dietz, T. Nicolay, J. Schmid, M. Schmidt, J. Bahnmueller, B. Kessler, B. Schuermann, and M. G. Mueller. Process monitoring or process control in laser materials processing. In *Proceedings of the 20th ICALEO*, volume 90, pages 1194–1200, Jacksonville, Florida USA, Oct. 15-18 2001.

[9] C. Kratzsch. *Realisierung eines kamerabasierten Prozessüberwachungssystems am Beispiel des Laserstrahlschweißens*. PhD thesis, RWTH Aachen, 2003.

[10] J.-R. Ohm. *Multimedia Communication Technology*. Springer, Berlin, 2004.

[11] A. Papoulis. *Probability & Statistics*. Prentice-Hall, Upper Saddle River, 1990.

[12] R. Poprawe. *Lasertechnik für die Fertigung*. Springer, Berlin, 2005.

[13] B. Regaard, S. Kaierle, W. Schulz, A. Moalem, Advantages of Coaxial External Illumination for Monitoring and Control of Laser Materials Processing. In *Proceedings of ICALEO*, paper #2307, pages 915–919, Miami, Florida USA, Oct. 31 - Nov. 3 2005.

[14] Z. Zhang. Parameter estimation techniques: A tutorial with application to conic fitting. Technical Report RR-2676, INRIA, Sophia Antipolis, 1995.